

Enhanced microwave absorption performance of MOF-derived hollow Zn-Co/C anchored on reduced graphene oxide

Yue Wang(王玥), Dawei He(何大伟), and Yongsheng Wang(王永生)
Citation: Chin. Phys. B, 2021, 30 (**6**): 067804. DOI: 10.1088/1674-1056/abd770
Journal homepage: http://cpb.iphy.ac.cn; http://iopscience.iop.org/cpb

What follows is a list of articles you may be interested in

Broadband microwave absorption properties of polyurethane foam absorber optimized by sandwiched cross-shaped metamaterial

Long-Hui He(贺龙辉), Lian-Wen Deng(邓联文), Heng Luo(罗衡), Jun He(贺君), Yu-Han Li(李宇涵), Yun-Chao Xu(徐运超), Sheng-Xiang Huang(黄生祥)
Chin. Phys. B, 2018, 27 (**12**): 127801. DOI: 10.1088/1674-1056/27/12/127801

Second harmonic generation of metal nanoparticles under tightly focused illumination

Jing-Wei Sun(孙经纬), Xiang-Hui Wang(王湘晖), Sheng-Jiang Chang(常胜江),Ming Zeng(曾明), Na Zhang(张娜)
Chin. Phys. B, 2016, 25 (**3**): 037803. DOI: 10.1088/1674-1056/25/3/037803

Synthesis and microwave absorption properties of graphene-oxide(GO)/polyaniline nanocomposite with gold nanoparticles

Fu Chen, He Da-Wei, WangYong-Sheng, Fu Ming, Geng Xin, Zhuo Zu-Liang
Chin. Phys. B, 2015, 24 (**8**): 087801. DOI: 10.1088/1674-1056/24/8/087801

Synthesis and microwave absorption properties of graphene-oxide(GO)/polyaniline nanocomposite with Fe_3O_4 particles

Geng Xin, He Da-Wei, Wang Yong-Sheng, Zhao Wen, Zhou Yi-Kang, Li Shu-Lei
Chin. Phys. B, 2015, 24 (**2**): 027803. DOI: 10.1088/1674-1056/24/2/027803

Enhanced microwave absorption performance of MOF-derived hollow Zn-Co/C anchored on reduced graphene oxide*

Yue Wang(王玥), Dawei He(何大伟)†, and Yongsheng Wang(王永生)

Key Laboratory of Luminescence and Optical Information, Ministry of Education, Institute of Optoelectronic Technology, Beijing Jiaotong University, Beijing 100044, *China*

(Received 8 December 2020; revised manuscript received 23 December 2020; accepted manuscript online 30 December 2020)

Composite materials assembled by metal/carbon nanoparticles and 2D layered flakes can provide abundant interfaces, which are beneficial for high-performance microwave absorbers. Herein, Zn-Co/C/RGO composites, composed of Zn-Co metal-organic framework-derived Zn-Co/C nanoparticles and reduced graphene oxide (RGO), were obtained through a facile method. The multilayer structure was due to the introduction of hollow Zn-Co/C nanoparticles in the RGO sheets. Zn-Co/C nanoparticles provided abundant polarization and dipole centers on the RGO surface, which enhanced the microwave absorption abilities. Different concentrations of RGO were introduced to optimize impedance matching. The minimum reflection loss (R_L) of Zn-Co/C/RGO with a thickness of 1.5 mm reached −32.56 dB with the bandwidth corresponding to R_L at −10 dB, which can reach 3.92 GHz, while a minimum R_L of −47.15 dB at 11.2 GHz was also obtained at a thickness of 2.0 mm. The electromagnetic data demonstrate that Zn-Co/C/RGO presented excellent absorption performance and has potential for application in the microwave absorption field.

Keywords: microwave absorption, metal nanoparticles, metal-organic framework (MOF), reduced graphene oxide

PACS: 78.30.Jw **DOI:** 10.1088/1674-1056/abd770

1. Introduction

The development of modern society is inseparable from technology and electronic science.[1–3] With the popularity of electronic devices, electromagnetic radiation pollution has become an urgent issue.[4–6] In order to protect human beings and high-end devices from electromagnetic radiation, finding a microwave absorbing material with high performance has received significant attention. Therefore, it is necessary to research effective microwave absorbers with strong microwave absorption, low cost, light weight, thin thickness and broad absorption bandwidth.[7–11]

The well-known carbon-based microwave absorbing agents such as graphene and carbon nanotubes are good light-weight dielectric absorbers.[12–19] Recently, GO as a traditional microwave absorber has been used as an ideal candidate due to its 2D structure, low density, abundant surface defects and high specific surface area.[20–23] However, the high conductivity and dielectric constant cannot meet the need for impedance matching, which causes the poor properties of attenuation and strong skin reflection of microwaves.[24,25] Therefore, numerous methods have been researched to rationally synthesize and change the structure of GO composites.[26–30] Several materials such as metals and ferrites can be applied to improve the structure and microwave absorption of GO. Previous studies have also shown that by the combination of GO with magnetic metallic nanoparticle materials, its relative permittivity and permeability can achieve the maximum absorption of microwave in a wide frequency range.[31] Li *et al.* combined the CeO_{2-x} with GO, which greatly improves its microwave absorption abilities and the minimum R_L is −50.6 dB.[32]

Metal-organic framework (MOF) materials are a kind of recently developed coordination compound composed of metal-coordinating clusters and aromatic organic linkers, which have proved to be an ideal precursor for inorganic materials.[33,34] Moreover, MOFs are considered to be an ideal metal/carbon precursor for fabricating metal/carbon composites by converting organic ligands and metal ions into carbon and metallic materials with a thermal annealing process.[35,36] In particular, MOFs containing magnetic metal ions are considered to be ideal precursors for preparing microwave absorbers.[37,38] Furthermore, the combination of MOF-derived hybrids such as ZIF with dielectric composites has been shown to be an available method for improving the microwave absorption properties of RGO.[39–41] For example, Wang *et al.* have shown that Co@C@RGO composite used Co-MOF as a precursor and produced excellent microwave absorption abilities with a minimum reflection loss (R_L) of −67.5 dB and effective absorption bandwidth of 5.4 GHz.[42] Using ZIF-67 as a template, Wang *et al.* developed carbon/Co/Co_3O_4/CNTs/RGO composites and achieved an excellent R_L performance of −59.2 dB with an

*Project supported by the National Key R&D Program of China (Grant No. 2016YFA0202302), the National Natural Science Foundation of China (Grant Nos. 61527817, 61875236, 61905010, and 61975007), and Beijing Natural Science Foundation, China (Grant No. Z190006).

†Corresponding author. E-mail: dwhe@bjtu.edu.cn

© 2021 Chinese Physical Society and IOP Publishing Ltd

absorption bandwidth of 5.7 GHz.[43] Relevant studies on 3D graphene-based composites have shown that the combination of RGO with N-doped CNTs and alloy composites or MOF-derived metallic nanoparticles provided abundant heterostructure interface, which caused more polarization loss.[44,45] The multi-layered RGO prevents the agglomeration of nanoparticles. At the same time, the metallic nanoparticles serving as the supporting point between the RGO layers also provide the re-stacking of RGO, which increases the reflection loss inside the material and enhances the microwave absorption capacity.[46,47]

As a traditional carbon-based microwave absorber, RGO has a large conductive network and specific surface area, but its shortcomings such as easy accumulation limit its practical application. The application of MOF with Fe, Co, Ni, Zn and other metal elements as the center in the field of microwave absorption has been extensively studied. In particular, some MOFs have good 3D structure and the combination with RGO can optimize the microwave absorption performance. In this study, Zn-Co/C/RGO nanocomposites derived from Zn-Co-MOF were obtained through a facile method. The as-prepared composite material has the following advantages: 1) the Zn-Co/C nanoparticles with hollow structure anchored on the RGO sheets, which assemble 2D RGO into 3D multi-interface structure and increase the reflection of microwaves inside the nanocomposites; 2) significant interfacial and dipole polarization and 3D conductive network induced by the special structure; 3) different RGO concentrations were used to adjust the impedance matching of these materials in order to enhance the microwave absorption abilities at low thickness. The minimum reflection loss value of −47.15 dB at 11.2 GHz was acquired when the thickness was 2.0 mm and the bandwidth at R_L equal to −10 dB can reach 3.5 GHz.

2. Experimental details

2.1. Materials

Cobalt nitrate hexahydrate ($Co(NO_3)_2{\cdot}6H_2O$), zinc nitrate hexahydrate ($Zn(NO_3)_2{\cdot}6H_2O$), isophthalic acid (H_2IPA), N,N-dimethylformamide (DMF) absolute ethanol and ascorbic acid were obtained commercially (Beijing Tong Guang Fine Chemicals Company).

2.2. Synthesis of Zn-Co/C nanoparticles

Zn-Co/C nanoparticles were prepared by the annealing of Zn-Co-based MOF precursors under Ar. The Zn-Co-based MOF precursors were prepared by a facile solvothermal method. Typically, 0.0464 g of $Co(NO_3)_2{\cdot}6H_2O$, 0.0472 g of $Zn(NO_3)_2{\cdot}6H_2O$ and 0.0528 g of isophthalic acid (H_2IPA) were dissolved in a mixture of N, N-dimethylformamide (25 ml) and anhydrous ethanol (25 ml) to form a clear solution by stirring for 4 h. The solution was transferred to a teflon-lined stainless-steel autoclave and kept at 160 °C for 4 h. After cooling to room temperature, the obtained Zn-Co-based MOF was separated by centrifugation. The Zn-Co/C nanoparticles were generated through thermal treatment of Zn-Co-based MOF in Ar at a temperature of 600 °C for 10 min.

2.3. Synthesis of Zn-Co/C/RGO

First, 30 ml solutions with different GO concentrations (0.6, 0.9, 1.2 and 1.5 mg/ml) were prepared by Hummers method.[48] After stirring for 1 h, 0.12 g of Zn-Co/C nanoparticles was added and ultrasonicated for 1 h. Then, 0.3 g of ascorbic acid was added and ultrasonicated for another 1 h. The solution was heated at 90 °C for 2 h. The samples were collected after centrifugation and dried for 12 h by lyophilization. The samples were termed ZC@G 1–4 (0.6, 0.9, 1.2 and 1.5 mg/ml), respectively.

2.4. Measurements

Scanning electron (SEM; SU8010) and transmission electron microscopies (TEM; JEM-1400) were used to observe the morphologies of samples. Powder x-ray diffraction (XRD; Co-$K\alpha$ radiation) and Fourier transform infrared spectroscopy (FTIR; Alpha) were used to characterize the elements and structure of the material. X-ray photoelectron spectrometry (XPS; Thermo Scientific) was used to study the photoelectron spectra.

The sample was mixed with paraffin and pressed into a ring shape (mass ratio of 20%, thickness of 2 mm, inner diameter and outer diameter of 3.04 and 7 mm) to measure the electromagnetic parameters. An Agilent E5071C vector network analyzer was used to characterize the electromagnetic parameters of the composite materials in the frequency range of 2–18 GHz. R_L was calculated using the following formula:

$$R_L = 20\lg\left|\frac{Z_{in}-1}{Z_{in}+1}\right|, \tag{1}$$

$$Z_{in} = \sqrt{\mu_r/\varepsilon_r}\tanh\left[j\left(2\pi f d/c\right)\sqrt{\mu_r\varepsilon_r}\right], \tag{2}$$

where Z_{in} is the input impendence, ε_r is the complex permittivity, μ_r is the complex permeability, f is the microwave frequency, d is the layer thickness, and c is the microwave velocity in free space.

3. Results and discussion

The micro morphology and structure of ZC@G3 were observed by SEM and TEM (Fig. 1). As shown in Fig. 1(a), the Zn-Co/C nanoparticles present a hollow structure with a size distribution at 800–1000 nm and Zn-Co-based MOF in Fig. 1(a) indicated its porous hollow structure. It can be seen from Fig. 1(b) that Zn-Co/C nanoparticles grow uniformly on

the surface of RGO. Fig. 1(d) also shows similar characteristics. The RGO sheets can effectively prevent the agglomeration of Zn-Co/C nanoparticles and enhance the microwave absorption properties by increasing the contact interface with the microwave.

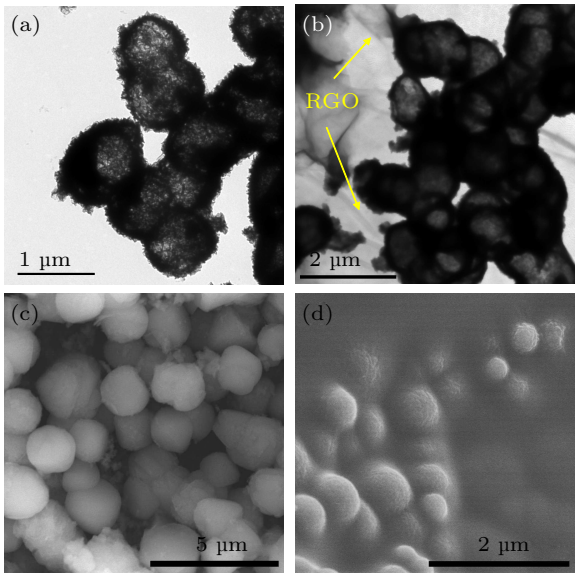


Fig. 1. TEM and SEM of Zn-Co/C ((a) and (c)) and Zn-Co/C/RGO ((b) and (d)).

As shown in Fig. 2(a), the components of the composites are identified through FTIR spectroscopy. The characteristic peaks at 1690 cm^{-1} and 1674 cm^{-1} are due to the skeleton vibrations of the aromatic ring. The vibration peaks at 1279 cm^{-1}, 1211 cm^{-1} and 1583 cm^{-1} can be attributed to the C=O stretching vibration and the peak at 765 cm^{-1} was due to the out-of-plane bending vibration of C–H. Those peaks identified that the band of C=O stretching vibration shifts from 1510 cm^{-1} to 1583 cm^{-1} after the formation of Zn-Co/C, demonstrating the coordination of carboxylate groups of H_2IPA to Co^{2+} and Zn^{2+} cations.[49]

Crystal phase compositions of ZC@G1-4 were analyzed by XRD (Fig. 2(b)). Diffraction peaks located at $2\theta = 10.8°$, 17.6° and 20.7° corresponded to (111), (220) and (311) reflection of C60, respectively.[50] These peak locations for C60 corresponded with the recorded XRD pattern (JCPDS No. 44-0558), suggesting the benzene ring structure in the organic ligand formed a spherical shape after annealing. For RGO, a weak diffraction peak located at 25.6° corresponded to the (002) plane of amorphous carbon.[51] The characteristic diffraction peaks at 44.3° and 75.9° coincide with the (111) and (220) crystal planes of metallic cobalt with face-centered cubic structure.[52] A diffraction peak observed at 43.2° corresponded to the (101) crystal planes of metallic zinc (JCPDS No. 87-0713).[53]

Detailed elemental compositions of ZC@G1-4 were determined by XPS spectra (Fig. 3). In the XPS full-spectrum, four peaks appearing at 284.4, 533.1, 778.08 and 1023 eV (Fig. 3(a)) correspond to the bond energies of C, Co and Zn, respectively. In the C 1s spectrum (Fig. 3(b)), the peaks distributed at 284.4 eV, 285.88 eV, and 288.2 eV correspond to C–OH and C=O, respectively.[54] The peaks at 777.88 eV and 793.08 eV were attributed to the Co $2p^{3/2}$ and Co $2p^{1/2}$, suggesting the existence of metallic Co and a small amount of Co^{2+}-O, probably due to the formation of Co oxide during the annealing process (Fig. 3(c)).[55,56] In the spectrum of Zn, the peaks at 1021.8 and 1044.98 eV were ascribed to Zn $2p^{3/2}$ and Zn $2p^{1/2}$, respectively (Fig. 3(d)).[57] Moreover, the weak peak intensity of Co 2p and Zn 2p suggested that most Zn-Co/C nanoparticles were covered with the RGO sheets.

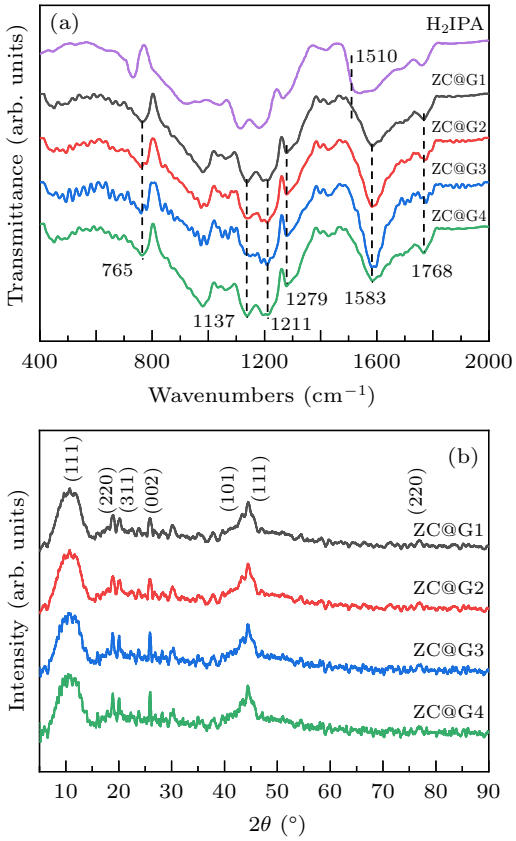


Fig. 2. FTIR (a) and XRD (b) patterns of Zn-Co/C/RGO.

The microwave absorption performance is related to the electromagnetic parameters and the microwave absorption mechanism can also be analyzed through the electromagnetic parameters. The electromagnetic parameters and loss angle of ZC@Gs are shown in Fig. 4. The real part of the complex permittivity (ε') and complex permeability (μ') represents the energy storage capacity, and the imaginary part of the relative complex permittivity (ε'') and relative complex permeability (μ'') is related to the loss capacity. As the increase of polarization relaxation phenomenon, the ε' of ZC@Gs decreased with the increasing frequency (Fig. 4(a)). Compared with Zn-Co/C (Fig. S1), the introduction of RGO has significantly increased the values of ε' and ε'', which was attributed to the excellent conductivity of RGO (Figs. 4(a) and 4(b)). Among the four

samples, ZC@G4 has the highest concentration of RGO, thus exhibiting the greatest conductivity. Likewise, $\tan\delta\varepsilon = \varepsilon'/\varepsilon''$ of ZC@G4 is greater than that of ZC@G1–3 (Fig. 4(c)). This indicates that ZC@G4, compared to other samples, exhibits higher storage and loss capability for electric energy. In contrast, the μ' and μ'' values of the four samples were all in the lower range, with μ' ranging from 1.05–0.95 (Fig. 4(d)), while μ'' was almost zero (Fig. 4(e)). The relative permeability of the four samples has similar obvious resonance peaks in the 2–18 GHz frequency range, indicating that the magnetic loss comes from the natural resonance and exchange resonance provided by the Zn-Co/C magnetic nanoparticles. The value

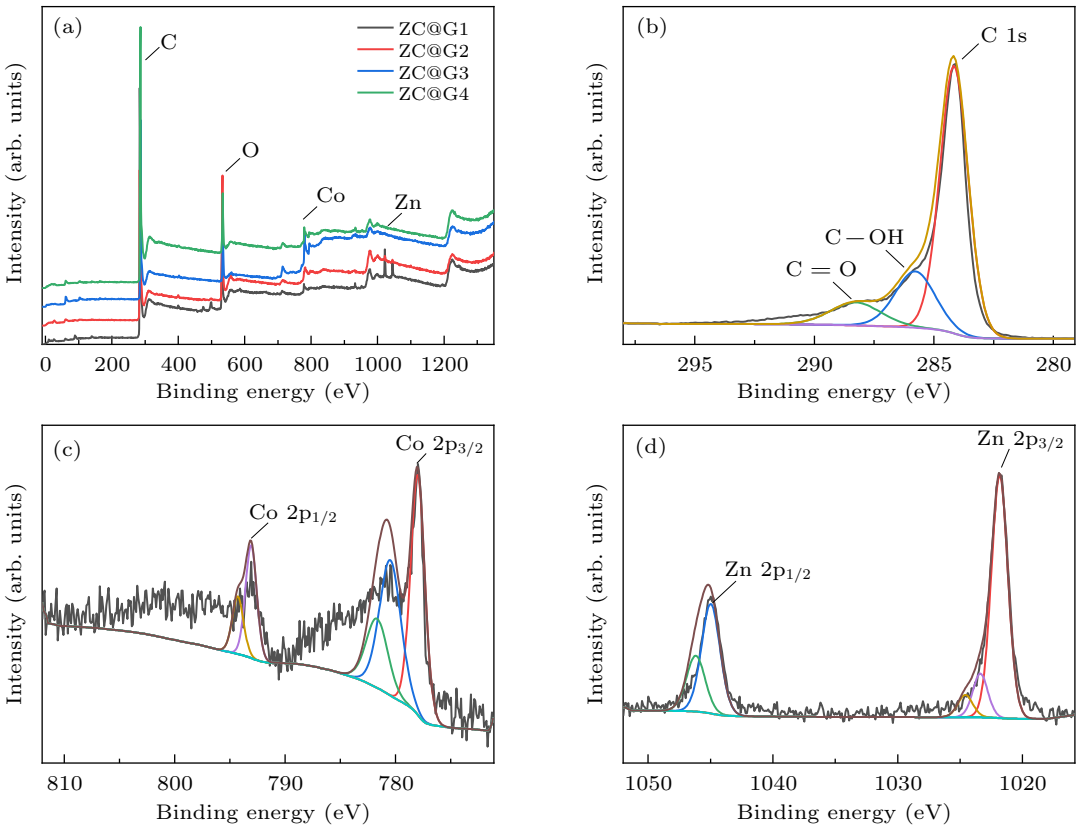


Fig. 3. XPS spectra of ZC@G1–4 (a), C (b), Co (c) and Zn (d).

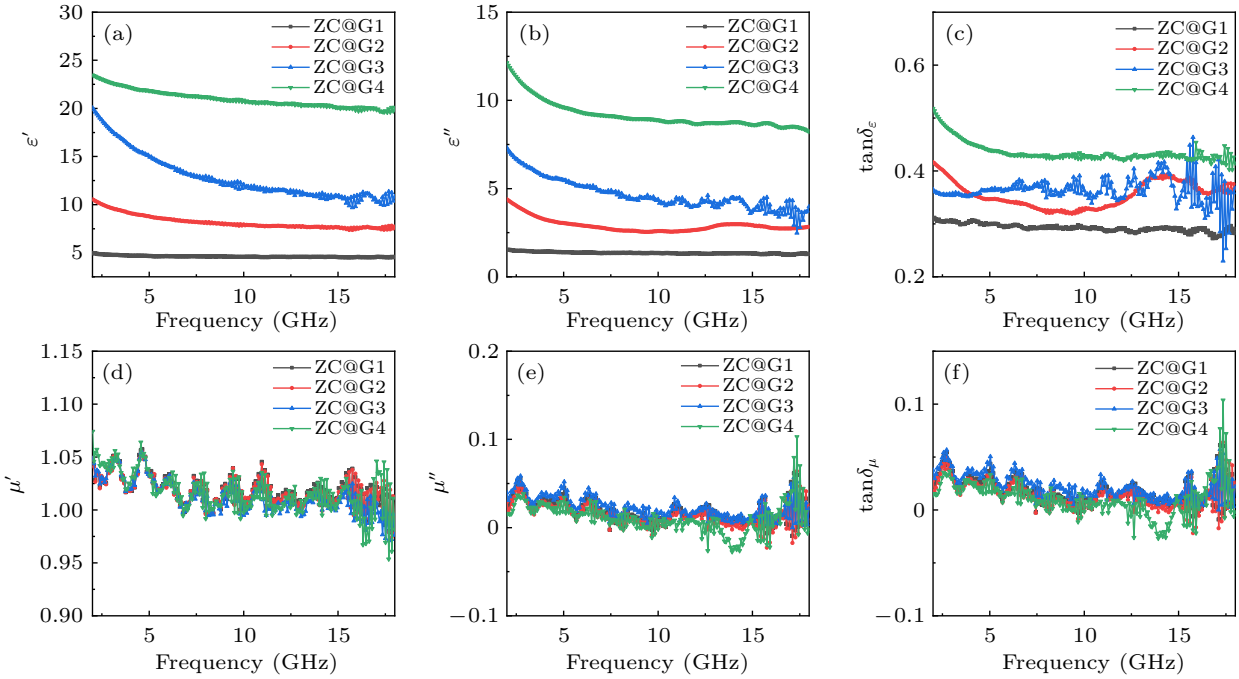


Fig. 4. Real parts (a) and imaginary parts (b) of permittivity, electric loss (c), real parts (d) and imaginary parts (e) of permeability and magnetic loss (f) for Zn-Co/C/RGO with different RGO content.

of μ'' was much smaller than ε'' of the four samples, indicating that the electrical loss played a major role in microwave absorption, which was also shown by the loss angle. The dielectric loss angle was significantly higher than the magnetic loss angle (Figs. 4(c) and 4(f)).

We characterize the microwave absorption capacity by calculating the R_L value (Fig. 5). It can be seen that ZC@G1, which has the smallest RGO mass ratio, exhibited poor microwave absorption capacity with a minimum R_L of −11.7 dB. With the increase of RGO mass ratio, ZC@G2 exhibited better microwave absorption capability; the minimum R_L is −24.3 dB at 14.0 GHz with a thickness of 2.0 mm. With the further increase of RGO concentration, ZC@G3 showed the best microwave absorption performance; at a thickness of 2.0 mm, the minimum R_L reached −47.15 dB at 11.2 GHz. Moreover, the minimum R_L of ZC@G3 is below −20 dB at thicknesses from 0.5 to 5.5 mm. More than 90% of the microwaves can be absorbed when R_L is lower than −10 dB and a value of R_L lower than −20 dB indicates more than 99% absorption of the microwaves. The minimum R_L of ZC@G1–4 is −10.67 (17.36), −24.30 (14.0), −47.15 (11.2) and −13.51 dB (8.16 GHz) at a thickness of 2.0 mm, respectively. With the increase of RGO content, the frequency corresponding to the minimum R_L shifts to a lower frequency, which indicated that the microwave absorption capacity of the absorber can be adjusted by controlling the RGO content. The absorption bandwidth is also an important aspect of the absorber. When the ZC@G1–4 thickness is 2.0 mm, the bandwidth corresponding to −10 dB is 0.96 (17.04–18), 4.08 (12.24–16.32), 3.52 (9.6–13.12) and 1.44 GHz (7.44–8.88 GHz).

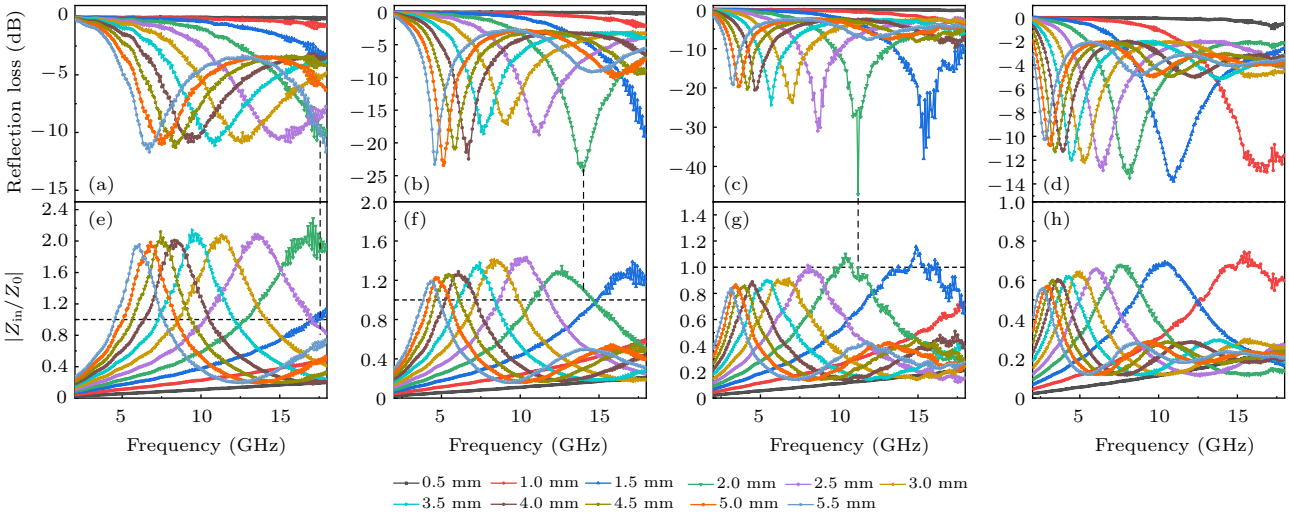


Fig. 5. Frequency dependence of the microwave reflection loss (R_L) curves and the modulus of the normalized characteristic impedance ($|Z_{in}/Z_0|$) curves of ZC@G1 (a), ZC@G2 (b), ZC@G3 (c) and ZC@G4 (d) in the frequency range of 2–18 GHz.

Zn-Co/C nanoparticles provide magnetic loss for the material. When the microwave interacts with it, the magnetic flux and magnetic induction intensity inside the Zn-Co/C/RGO will change and the eddy current will be formed inside the material, which converts the microwave into heat and consumes it. The magnetic loss mechanism of the material can be analyzed by the C_0 curve, which can be calculated by the following formula:

$$C_0 = \mu''(\mu')^{-2} f^{-1}.$$

When C_0 approaches constant, this indicates that the magnetic loss of the material is mainly provided by the eddy current loss of the nanoparticles. As shown in Fig. S4, in the 5–18 GHz frequency range, C_0 almost approaches constant, which indicates that the eddy current loss provided by Zn-Co/C nanoparticles plays an important role in microwave absorption.

The attenuation constant is usually used to evaluate the properties of microwave absorption, which can be calculated by the following formula:

$$\alpha = \frac{\sqrt{2}\pi f}{c} \times \sqrt{(\mu_r''\varepsilon_r'' - \mu_r'\varepsilon_r') + \sqrt{(\mu_r''\varepsilon_r'' - \mu_r'\varepsilon_r')^2 + (\mu_r''\varepsilon_r'' + \varepsilon_r')^2}}. \quad (3)$$

The α increased with the increase of RGO content, which indicated that the introduction of RGO enhanced the energy attenuation of composites due to the high conductivity of RGO (Fig. S3). ZC@G4 has the highest absorption constant, indicating that this sample has the strongest microwave absorption capacity. However, higher dielectric constant results in more microwave reflection. The impedance matching is another important parameter of the microwave absorption properties. The impedance matching is calculated by the ratio of the incident impedance (Z_{in}) and free space (Z_0). According to the impedance matching principle, when the ratio of Z_{in} to Z_0 is equal to 1, no microwave will be reflected when interacting with the material surface. As shown in Figs. 5(e)–5(h), the $|Z_{in}/Z_0|$ of ZC@G1 is far from 1, but with RGO mass ratio

increased, the $|Z_{in}/Z_0|$ of ZC@G2–4 is closer to 1 and finally lower than 1. For ZC@G3, the minimum of $|Z_{in}/Z_0|$ was close to 1 from 1.5 to 3.5 mm thickness and demonstrated better microwave absorption abilities than ZC@G1, 2 and 4, which was also shown through R_L (Fig. 5(c)).

Figure 6 reveals the microwave absorption mechanism of Zn-Co/C/RGO nanocomposites. The large heterointerface formed by Zn-Co/C nanoparticles anchored on RGO sheets improves the microwave energy attenuation by enhancing the interfacial polarization effect. Moreover, defects and functional groups that formed on RGO induced the formation of dipoles, which convert electromagnetic energy into heat energy. Furthermore, the introduction of RGO provided good resistance loss, which led to higher conductivity compared to the composite without RGO. The excellent microwave absorption performance of Zn-Co/C/RGO also benefits from the hollow structure of Zn-Co/C. The polarization centers produced by Zn and Co metal nanoparticles are distributed on the surface of Zn-Co/C, which provides the dielectric loss. The hollow structure also has an inner surface; hence it has more polarization centers than the solid material.[19] And inside the Zn-Co/C, microwaves are reflected between the inner surfaces, which increases the interaction between microwaves and the material and consequently improves the microwave absorption capacity of Zn-Co/C/RGO.

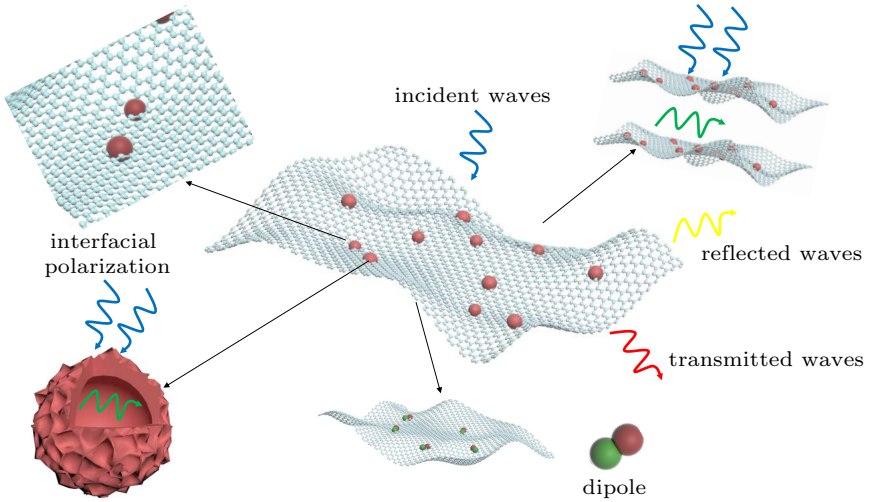


Fig. 6. Attenuation constant of ZC@G1, ZC@G2, ZC@G3 and ZC@G.

In conclusion, the excellent microwave absorption properties of Zn-Co/C/RGO nanocomposites were mainly attributed to the following aspects. First, the introduction of Zn-Co/C nanoparticles optimized 2D graphene into a composite with 3D structure. At the same time, the thin layer of RGO also prevented Zn-Co/C from agglomeration, thereby further increasing the contact surface. Second, when the incident microwave interacted with the material, the adjustable impedance matching enabled the microwave to enter the absorber effectively. Third, the hollow porous structure of Zn-Co/C nanoparticles had more polarization centers and provided a large amount of relaxation loss, while the RGO provided a conductive network as a carrier of electron transport, which enhanced the microwave loss ability.

4. Conclusion

In summary, Zn-Co/C/RGO nanocomposite material with excellent microwave absorption properties was obtained through a simple solvothermal method. Zn-Co/C nanoparticles with hollow porous structure are anchored on the surface of RGO sheets. Under different RGO composite concentrations, the microwave absorption properties of Zn-Co/C/RGO composites were analyzed. The existence of RGO increased the dielectric constant of the material, indicating that adjusting the content of RGO can control the impedance matching of the material. In addition, the conductive network provided by RGO increased the dielectric loss. Porous hollow Zn-Co/C nanoparticles and RGO sheets enhanced the interface and dipolar polarization. The Zn-Co/C/RGO composite material exhibited excellent microwave absorption capability at low thickness. At a thickness of 2.0 mm, the minimum R_L can reach −47.15 dB, with a bandwidth of 3.5 GHz. At a thickness of 1.5 mm, the minimum R_L of −32.56 dB can also be obtained. Within the thickness range of 1.5–5.5 mm, the minimum R_L is lower than −20 dB. Therefore, it is believed that this Zn-Co/C/RGO nanocomposite material with excellent microwave absorption capacity has good application prospect in the field of microwave absorption.

References

[1] Green M and Chen X 2019 *Journal of Materiomics* **5** 503

[2] Liu L, Wang L, Li Q, Yu X, Shi X, Ding J, You W, Yang L, Zhang Y and Che R 2019 *ChemNanoMat* **5** 558
[3] Zhao Z, Xu S, Du Z, Jiang C and Huang X 2019 *ACS Sustainable Chem. Eng.* **7** 7183
[4] Liu H, Li L, Wang X, Cui G and Lv X 2020 *Materials* **13** 4527
[5] Sun Q, Cai Y, Sun L, Ye W, Long X, Xu S, Ji Y and Wang R 2020 *Journal of Materials Science* **56** 1492
[6] Uddin W, Rehman S U, Aslam M A, Rehman S U, Wu M and Zhu M 2020 *Materials Research Bulletin* **130** 110943
[7] Wang H, Shi P, Rui M, Zhu A, Liu R and Zhang C 2020 *Progress in Organic Coatings* **139** 105476
[8] Wang S, Jiao Q, Liu X, Xu Y, Shi Q, Yue S, Zhao Y, Liu H, Feng C and Shi D 2019 *ACS Sustainable Chem. Eng.* **7** 7004
[9] Liu J, Che R, Chen H, Zhang F, Xia F, Wu Q and Wang M 2012 *Small* **8** 1214
[10] Liu Q, Cao Q, Bi H, Liang C, Yuan K, She W, Yang Y and Che R 2016 *Adv. Mater.* **28** 486
[11] You W, Bi H, She W, Zhang Y and Che R 2017 *Small* **13** 1602779
[12] Wang X, Huang L, Li J, Du Y, Wang Q, He X and Yuan Y 2020 *J. Appl. Phys.* **127** 205102
[13] Ma J, Li W, Fan Y, Yang J, Yang Q, Wang J, Luo W, Zhou W, Nomura N, Wang L and Jiang W 2019 *ACS Appl. Mater. Interfaces* **11** 46386
[14] Zhou E, Xi J, Guo Y, Liu Y, Xu Z, Peng L, Gao W, Ying J, Chen Z and Gao C 2018 *Carbon* **133** 316
[15] Zhao H, Yeow Seow J Z, Cheng Y, Xu Z J and Ji G 2020 *Ceramics International* **46** 15447
[16] Yan L, Zhang M, Zhao S, Sun T, Zhang B, Cao M and Qin Y 2020 *Chemical Engineering Journal* **382** 122860
[17] Che R C, Peng L M, Duan X F, Chen Q and Liang X L 2004 *Adv. Mater.* **16** 401
[18] Che R C, Zhi C Y, Liang C Y and Zhou X G 2006 *Appl. Phys. Lett.* **88** 033105
[19] Yan F, Guo D, Zhang S, Li C, Zhu C, Zhang X and Chen Y 2018 *Nanoscale* **10** 2697
[20] Fu C, He D, Wang Y and Zhao X 2019 *Synthetic Metals* **257** 116187
[21] Bai Y W, Shi G, Gao J and Shi F N 2020 *Journal of Solid State Chemistry* **288** 121401
[22] Sun H, Che R, You X, Jiang Y, Yang Z, Deng J, Qiu L and Peng H 2014 *Adv. Mater.* **26** 8120
[23] Wu Z, Pei K, Xing L, Yu X, You W and Che R 2019 *Advanced Functional Materials* **29** 1901448
[24] Zong H, Yang H, Dong J, Ma L, Lin Y, Qiu Y and Wen B 2020 *J. Mater. Sci: Mater. Electron.* **31** 18590
[25] Wu Z, Huang T, Li T and Li L 2019 *Langmuir* **35** 3688
[26] Kang Y, Yuan B, Ma T, Chu Z Y and Zhang Z J 2018 *J. Inorg. Mater.* **33** 1259
[27] Yu W Q, Qiu Y C, Xiao H J, Yang H T and Wang G M 2019 *Chin. Phys. B* **28** 108103
[28] Wanga X, Lua Y, Zhua T, Changa S and Wang W 2020 *Chemical Engineering Journal* **388** 124317
[29] Wang Y, Suo B, Shi Y, Yuan H, Zhu C and Chen Y 2020 *ACS Appl. Mater. Inter.* **12** 40692
[30] Zhang X, Yan F, Zhang S, Yuan H, Zhu C, Zhang X and Chen Y 2018 *Appl. Mater. Inter.* **10** 24920
[31] Zhang X, Xu J, Yuan H, Zhang S, Ouyang Q, Zhu C, Zhang X and Chen Y 2019 *Appl. Mater. Inter.* **11** 39100
[32] Li Q, Zhao Y, Li X, Wang L, Li X, Zhang J and Che R 2020 *Small* **16** 2003905
[33] Huo J, Wang L and Yu H 2009 *Journal of Materials Science* **44** 3917
[34] Ruan W, Mu C, Wang B, Nie A, Zhang C, Du X, Xiang J, Wen F and Liu Z 2018 *Nanotechnology* **29** 405703
[35] Wang L, Wen B, Yang H, Qiu Y and He N 2020 *Compos Part A: Appl. S.* **135** 135958
[36] Zhang Y, Zhang H B, Wu X, Deng Z, Zhou E and Yu Z Z 2019 *ACS Applied Nano Materials* **2** 2325
[37] Liu D, Du Y, Wang F, Wang Y, Cui L, Zhao H and Han X 2020 *Carbon* **157** 478
[38] Liu W, Shao Q, Ji G, Liang X, Cheng Y, Quan B and Du Y 2017 *Chemical Engineering Journal* **313** 734
[39] Gupta S, Chang C, Anbalagan A K, Lee C H and Tai N H 2020 *Composites Science and Technology* **188** 107994
[40] Hu Q, Qi X, Cai H, Xie R, Long L, Bai Z, Jiang Y, Qin S, Zhong W and Du Y 2017 *Sci. Rep.* **7** 11213
[41] Li X, Wang L, Li X, Zhang J, Wang M and Che R 2021 *Carbon* **172** 15
[42] Wang Y, Di X, Gao X and Wu X 2020 *Nanotechnology* **31** 395710
[43] Wang Y, Di X, Wu X and Li X 2020 *J. Alloys Compd.* **20** 156215
[44] Xu J, Zhang X, Yuan H, Zhang S, Zhu C, Zhang X and Chen Y 2020 *Carbon* **159** 357
[45] Zhang X, Xu J, Liu X, Zhang S, Yuan H, Zhu C, Zhang X and Chen Y 2019 *Carbon* **155** 233
[46] Zhang X, Zhang X, Wang D, Yuan H, Zhang S, Zhu C, Zhang X and Chen Y 2019 *Journal of Materials Chemistry C* **7** 11868
[47] Zhang X, Zhang X, Yuan H, Li K, Ouyang Q, Zhub C, Zhanga S and Chen Y 2020 *Chemical Engineering Journal* **383** 123208
[48] Hummers W S Jr. and Offema R E 1958 *J. Am. Chem. Soc.* **80** 1339
[49] Guan B Y, Kushima A, Yu L, Li S, Li J and Lou X W D 2017 *Adv. Mater.* **29** 17
[50] Atamny E, Baiker A, Muhr H J and Nesper R 1995 *Fresenius J. Anal. Chem.* **353** 433
[51] Fan X, Zhang A, Li M, Xu H, Xue J, Ye F and Cheng L 2020 *Journal of Materials Science: Materials in Electronics* **31** 11774
[52] Sun Y, Jia H, Liu J, Yu H and Jiang X 2020 *Journal of Materials Science: Materials in Electronics* **31** 11700
[53] Miao P, Cao J, Kong J, Li J, Wang T and Chen K J 2020 *Nanoscale* **12** 13311
[54] Peng C, Zhang Y and Zhang B 2020 *J. Alloys Compd.* **826** 154203
[55] Lu Y, Wang Y, Li H, Lin Y, Jiang Z, Xie Z, Kuang Q and Zheng L 2015 *ACS Appl. Mater. Interfaces* **7** 13604
[56] Ding D, Wang Y, Li X, Qiang R, Xu P, Chu W, Han X and Du Y 2017 *Carbon* **111** 722
[57] Ma T, Cui Y, Sha Y, Liu L, Ge J, Meng F and Wang F 2020 *Synthetic Metals* **265** 116407